

Mechanical testing and numerical simulations on fatigue behavior of a clad Al/Al-Mg alloy

C. Zhang¹, Y. Y. Teng², W. Liu^{1,2*}, L. Lin², X. X. Hu³, Y. H. Jiang³, X. Y. Ye¹, M. W. Zhou⁴, J. W. Wang⁵

¹*School of Information and Intelligent Engineering, Zhejiang Wanli University, Ningbo 315100, P. R. China*

²*Zhejiang University, Hangzhou 310000, P. R. China*

³*Xingyu Electron (Ning Bo) Co., Ltd., Ningbo 315100, P. R. China*

⁴*Ningbo Zhenyu Technology Co., Ltd., Ningbo 315100, P. R. China*

⁵*Ningbo Shuanglin Auto Parts Co., Ltd., Ningbo 315100, P. R. China*

Received 18 March 2021, received in revised form 25 June 2021, accepted 22 July 2021

Abstract

This work presents mechanical testing and numerical simulations on fatigue behavior, particularly the fatigue life and failure modes and the final fracture of metallic materials. First, the mechanical tests of the base alloys and their welded joint were conducted, and the stress-circulation curve with a survival rate was obtained. Second, the failure modes and fracture mechanisms of such metallic materials were analyzed. Third, the load spectrum of the key parts of a typical welding joint was converted into a stress spectrum. Finally, the fatigue life of the components was achieved based on the finite element analysis and corresponding numerical simulations. The results showed a very promising application of such composite materials to meet the safety requirements. Therefore, the present study also provides an efficient method, which can be applied in various industrial aspects such as materials and mechanical engineering, as well as structural control and safety monitoring.

Key words: finite element method, aluminum alloy, deformation behavior, fatigue properties

1. Introduction

The demand for transporting concentrated nitric acid and a limited railway transportation capacity requires the use of large-capacity tank cars. In this study, the use of a 70-t tank car to transport concentrated nitric acid is considered an alternative to the use of the existing 60-t tank car to improve transportation efficiency [1, 2]. Considering the factors of low weight and corrosion prevention, high-strength clad plates can be used to meet the above requirements of materials for the tank car body. A thin pure aluminum layer used for the internal bladder material of the tank body reacts with the concentrated nitric acid to produce a layer of oxide film that protects the layer. The thicker layer is the outer layer material and bears the external load. The pure metals and their alloys form a clad plate through a solid-state com-

ination. However, only an alloy can be used as the butt weld filler material of the clad plate, and this exposes a small amount of alloy filler on the pure aluminum layer to the concentrated nitric acid. Therefore, it is necessary to lap the alloy cover on one side of the pure aluminum layer of the butt weld of the clad plate to ensure the corrosion protection of the tank body material.

The safe and stable operation of transformers plays an important role in the power system. The box joint of the bell jar tank is welded. For welded joints, the sealing mechanism is to seal by welding the upper and lower joints together to form a closed whole. Due to the welding connection, the stress the welding location can bear is lower than the yield strength of the casing joint materials (the maximum stress is less than 85 % of the yield strength of base materials). In particular, with the use of a transformer, the internal coil vibra-

*Corresponding author: e-mail address: larkxh@163.com

tion of the joint can cause fatigue, which will further reduce the stress limit value and lead to harmful effects on its use for lifting. If the transformer tank is hoisted, the joint will deform, and the stress on the joint will increase. When the stress reaches the limit value of the welding part, cracks and even oil leakage will occur.

Cladded metal composites (LMCs) are unique composites in which alternating metal or metal-containing layers are combined with discrete interfaces. LMCs significantly improve the performance of many materials in terms of fracture toughness, fatigue behavior, impact behavior, wear, corrosion, and damping capacity. These composites enhance the ductility of brittle materials and are widely used in the aerospace, automotive, and defense fields [3, 4]. The manufacturing process and mechanical properties of cladded plate materials are very different from traditional monolithic materials. Many researchers have conducted in-depth research on the manufacturing process, mechanical properties [5–9], and fatigue crack growth [10–15] of cladded plate materials. The study by Wittenauer and Sherby [10] showed that the fatigue life of an ultra-high carbon steel cladded plate containing a thin copper coating was significantly higher than that of the monolithic material. During the fatigue loading, the plastic deformation of the copper layer results in delamination, which causes blunt crack tips. The increase in the fatigue life is more apparent under high-amplitude stress cycles due to the growth of fatigue cracks. In the case of high-cycle fatigue, the fatigue life is determined by the initiation life of the crack, and the fatigue life of cladded materials is similar to that of monolithic material.

Kümmel et al. [11] studied the fatigue deformation and damage mechanism of cladded composites with distinct hardness differences. At high amplitudes, the cracks extended in the thickness direction and were not affected by the various interfaces in the cladded plate. At low amplitudes, a grain coarsening occurred in the layer, and the cracks extended along the direction of the layer, but this was not the case for the monolithic material. The fatigue life and cycle stability of a cladded plate are significantly higher than those of monolithic material. Pippan et al. [12] studied the crack growth of LMCs in detail. They found that if the fatigue crack approached the interface from the weaker plastic material, the crack growth rate decreased near the interface due to the change in the plastic deformation field at the crack tip, and the cracks began to branch. In contrast, the crack growth rate was accelerated when the cracks were close to the interface with the stronger plastic material. Cui et al. [13] studied the expansion of fatigue cracks in laminates with different bonding strength at the interface. Due to the influence of the interface microstructure and bonding strength, the stress state at the

crack tip changed from a plane strain state to a plane stress state; therefore, strain energy was released, and crack arrest occurred. According to the study of He et al. [14], the plastic deformation of the softer materials consumes the deformation energy and reduces the crack driving force, which agrees with the conclusion of Cui et al. [13]. Kolednic et al. [15] investigated the expansion of fatigue cracks in cladded plates with different hardness values. If the crack tip was located in a material with a low Young's modulus, the driving force of the crack was strongly reduced at the interface, which caused an arrest in the crack growth. Therefore, the material exhibited high fracture strength. The mechanical properties and low-cycle fatigue properties of cladded composites were investigated by Szachogluchowicz et al. [16, 17]. Huang et al. [18] found that an overload in the fatigue cycle had little effect on the crack growth rate of fiber-metal composites.

To sum up, current studies of the fatigue performance of LMCs are mainly based on theoretical research, and there are few studies on the fatigue performance of cladded plates and the welded joints using tests and practical engineering applications [18–20]. In this work, we present an experimental investigation and a finite element analysis on the mechanical behavior of transformer joint materials, particularly the fatigue performance, and provides an efficient method, which can be applied to transformer box seal monitoring and fault diagnosis.

2. Simulations

Because the material considered in this study is a metallic composite, the basic mechanical properties of the cladded plate are very important in the design of the tank car. Based on the parameters of the alloys, the ANSYS software is used to simulate a tensile test of a specimen of the cladded plate. The tensile test results provide the mechanical parameters of the base metals of the cladded plate to conduct a finite element analysis of the tank body.

2.1. Material parameters

The mechanical properties of the two materials are shown in Table 1 and are based on the standard GB/T 16475-1996 [21]. The constitutive relationships are simulated by ANSYS's bilinear hardening model BKIN, and it is apparent that the mechanical properties of the two materials are quite different.

2.2. Finite element model

The same specimen is analyzed in the fatigue test, and it has the same plate thickness as the actual application. A finite element model of the specimen is

Table 1. Tensile properties of 1060 aluminum and 5052 Al-Mg alloy at room temperature

Grade	State	Elastic modulus E (GPa)	Tensile strength σ_b (MPa)	Yield strength σ_y (MPa)	Elongation δ (%)	Hardness HBS
1060	O	69	69	25	43	19
5052	H32	69.3	230	195	12	60



Fig. 1. Loading method for the finite element analysis model of the specimen.

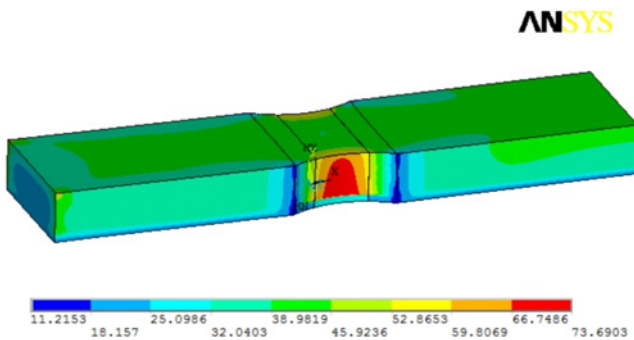


Fig. 2. Stress distribution of the model under a 4.6 t load.

created to simulate the elastoplastic stress and strain response of the specimen under a tensile load; the specimen is meshed using the solid element Solid45. To ensure the accuracy of the calculation results, the interface of the two kinds of materials and the arc area of the specimen are defined as key sites, and mesh refinement is performed to simulate the real material in the tensile test. All the nodes on the left side of the model are multi-constrained, and a displacement load of 2 mm is applied to the node on the right side. The specimen is then gradually loaded using sub-load steps, as shown in Fig. 1. Subsequently, the constraint reaction force at the left side of each load step is determined, and the nominal stress is calculated by dividing the cross-sectional area of the specimen arc. Finally, the stress and strain results of each load step are obtained.

2.3. Elastoplastic analysis

The equivalent stress, i.e., the ratio of von Mises stress versus the yield strength, of the specimen at a constraint force of 4.6 t, which corresponds to the tensile test load of 4.6 t (nominal stress of 46.45 MPa), is shown in Fig. 2. The stress concentration occurs at the outer surface of the specimen’s arc area, where the interface of the composite exhibits the highest stress of 73.69 MPa (lower than its yield strength). The pure aluminum layer has entered the yield state, and the stress is around 25 MPa.

The relationship between the maximum stress and the external load of the two materials can be described as follows: In the first stage, the two materials exhibit elastic deformation; this represents the stage in which the maximum stress $\sigma_{AL} < 25$ MPa. The two materials bear the load together. As the external load increases, the stress of the two materials increases linearly. In the second stage, the σ_{AL} remains at about 25 MPa. The maximum stress of the layer occurs in this stage at $\sigma_{AL-Mg} < 195$ MPa, and the load is mostly supported. As the external load increases, the stress of the pure layer remains basically unchanged, whereas the stress of the alloy layer increases linearly. In the third stage, both materials yield, namely, the σ_{AL-Mg} remains at 195 MPa and the σ_{AL} remains at 25 MPa. As the external load increases, the stress of the two materials remains basically the same. The external load $F = 173.49$ kN divided by the minimum cross-sectional area of the model results in nominal stress of $\sigma = F/A = 146.9$ MPa. It is considered that the clad plate yields when the pure aluminum layer yields. Therefore, the yield strength of the clad plate is 146.9 MPa. In the fourth stage, the two materials exhibit plastic deformation where $\sigma_{AL} > 25$ MPa and $\sigma_{AL-Mg} > 195$ MPa. The two materials are loaded simultaneously, but the load is mainly supported by the composite. As the external load increases, the stress of the two materials increases linearly, but the rate of increase is higher for the composite layer than for the pure aluminum layer.

The segment of the curves of both materials during the plastic phase is fitted using the least squares method. As shown in Fig. 3, the tensile strength is 98.7 MPa and 258 MPa, respectively, for the two materials. The alloy will break when the stress reaches 258 MPa because the external load is calculated as $F = 202.25$ kN according to the fitted equation, and

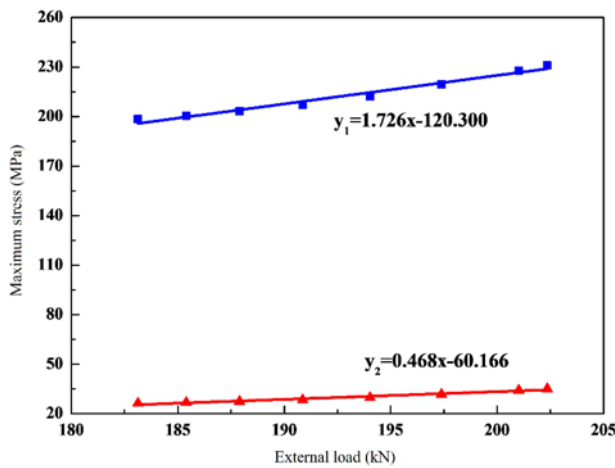


Fig. 3. Maximum stress vs. the external load during the plastic stage.

the nominal stress of the cladded plate is $\sigma = F/A = 171.3$ MPa.

Table 2 shows the test results of the tensile strength of the cladded plate, and the average value of the tensile strength is:

$$\bar{\sigma} = \sum_{i=1}^6 \sigma_i / 6 = 177.83 \text{ MPa.} \quad (1)$$

The result of the finite element calculation is close to the experimental result, which validates the elasto-plastic simulation results. In addition, since the yield

strength is 25 MPa and the yield strength of the alloy is 195 MPa, the tensile strength of the cladded plate is 171.3 MPa, and the yield strength ratio of the material is greater than 50 %. Therefore, the yield strength value of 146.9 MPa is a relevant result.

The mechanical performance parameters of the cladded plate obtained by the finite element simulation show a yield strength of $\sigma_s = 146.9$ MPa, a tensile strength of $\sigma_b = 171.3$ MPa, and a fracture strain of $\delta = 0.11$.

3. Fatigue tests

3.1. Specimens and loading conditions

The specimen has a symmetrical structure. As shown in Fig. 4, the length of the specimen is 240 mm, and the thickness is 22 mm. The specimen is divided into two layers. The upper layer is a pure aluminum layer with a thickness of 3 mm. The lower layer is the composite with a thickness of 19 mm. The two-layer material is consolidated to form a cladded plate. Because the boundary section of the two layers is too thin, one cannot see it clearly. The transition arc with a radius of 36 mm is located in the middle part of the specimen. The maximum cross-sectional area of the specimen is 1276 mm², and the minimum cross-sectional area is 990 mm².

The weld electrode type used is 5183. All the longitudinal and circumferential welds are butt weld joints with a 60-degree groove. After the front groove side is

Table 2. Tensile strength test results

Specimen number	1-26-1	1-26-2	1-26-3	2-26-1	2-26-2	2-26-3
Tensile strength (MPa)	196	189	186	166	166	164

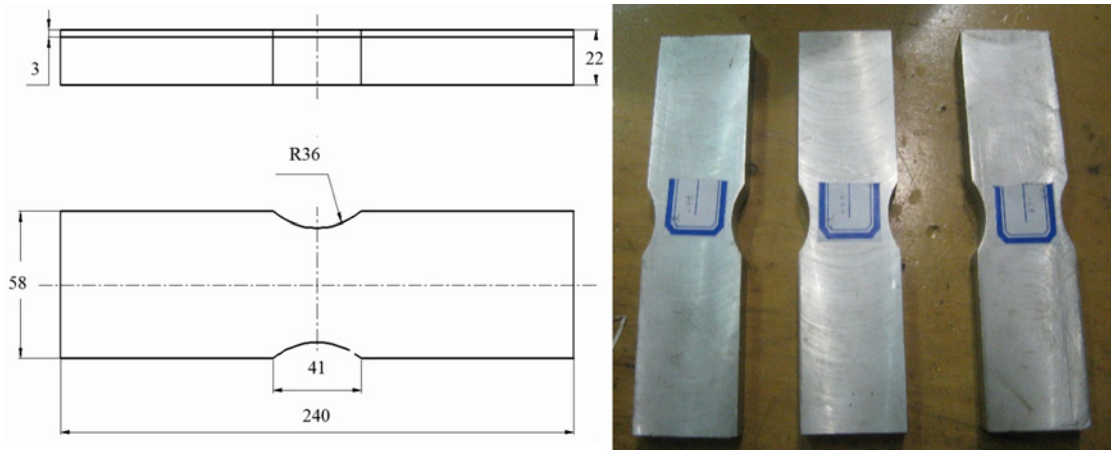


Fig. 4. Base metal specimen for the fatigue test.

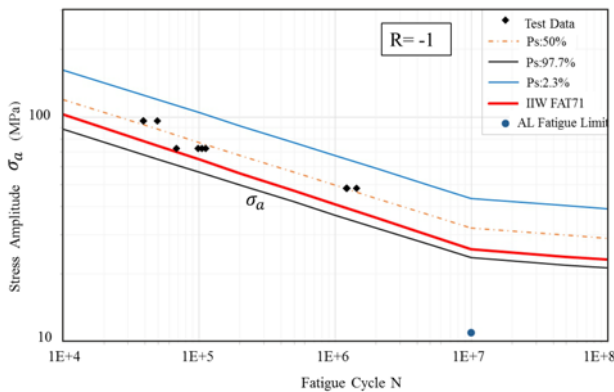


Fig. 5. S - N curves of the cladded plate for $R = -1$.

welded, the back groove bottom is cleaned before the back welding, which guarantees the double sides are fully penetrated. Then the pure aluminum cover plate is lap welded to protect the inside from corrosion; the local welded joint is the same as the lap-welded specimen used in the previous fatigue tests.

The test equipment is an MTS810 fatigue test system. The test system has a coaxial design, which results in a symmetrical force being applied to the specimen. The maximum allowable error of the average static and dynamic amplitude is no more than ± 1 and $\pm 3\%$, respectively. The test is carried out at room temperature at a frequency of 7 Hz. The fatigue tests were performed under a tension-pressure symmetrical cycle ($R = -1$), a zero-tension pulsation cycle ($R = 0$), and a zero-pressure pulsating cycle ($R = -\infty$); the test was terminated when the specimen fractured.

3.2. Test results and discussion

The test results are shown in Fig. 5. For $R = -1$, the slope of the median S - N curve is $k = 5.2$ based on regression analysis, and this is not a big difference from the slope of the S - N curve of the layer alloy. Usually, the logarithmic life of a specimen is normally distributed. The standard deviation $s = 0.0659$ of the life distribution is analyzed by the unilateral tolerance method, and it is close to the dispersion band in the International Institute of Welding (IIW) standard [21]. The composite cladded plates are metal materials essentially. The process of fatigue crack initiation and propagation should be experienced under cyclic loading. The test data before the $2e6$ cycle determine the trend of the S - N curve. Based on limited test data of this study, according to Sonsion [22] and Hobbacher [23], who conducted high-cycle fatigue research on layer alloy material, the S - N curve can be reasonably extended to the long-life range, and the knee point of the S - N curve is defined as the $1e7$ cycle. After the knee point, the fatigue strength decreases with the increase in the cycle times, and the

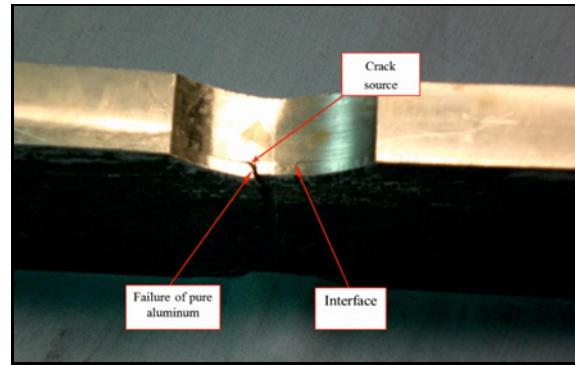


Fig. 6. The typical failure mode of the specimen.

slope changes to $k^* = 22$. At the same time, a curve with a survival rate of 97.7% can be obtained by subtracting 2 standard deviations from the median curve, and the fatigue limit at the $1e7$ cycle is 23.62 MPa.

In the IIW standard, the FAT value of the 5-line is 71 MPa, and the fatigue limit at the $1e7$ cycle is 25.73 MPa. In addition, according to the standard JB/T 4734-2002 for the welding containers [24] and the American Society of Mechanical Engineers (ASME) boiler and pressure vessel code volume II [25], the allowable stress of 1060 pure aluminum layer under annealing conditions is only 11 MPa. It is evident that the fatigue strength of the alloy cladded plate is much higher than that of the pure aluminum layer, which is close to the 5 series. Therefore, this material is sufficiently lightweight for use in a tank car carrying concentrated nitric acid.

3.3. Fatigue failure mode

The failure type of the specimens is shown in Fig. 6. The fatigue cracks of the cladded plate originate from the pure aluminum layer cross-section. This is due to the minimum constraint on the cyclic plasticity at the edge of the cross-section. In the fatigue test load, the yield strength of the pure aluminum layer is low, and it is prone to repeated plastic deformation. The stress of the composite is still in the elastic range; therefore, at the interface, the pure aluminum layer side cannot slip easily due to the deformation constraints of the composite, which results in the tension of the stress field and eventually leads to stratification. This area then becomes a weak zone prone to fatigue; the fatigue crack begins in the pure aluminum layer and after the formation of the fatigue crack and first extends along the direction of the pure aluminum layer along the cross-section. After destroying the pure aluminum layer, the crack extends along the transverse direction towards the composite, and the specimen finally fractures. The purpose of the $R = -\infty$ fatigue tests is to determine whether there is an interfacial instability

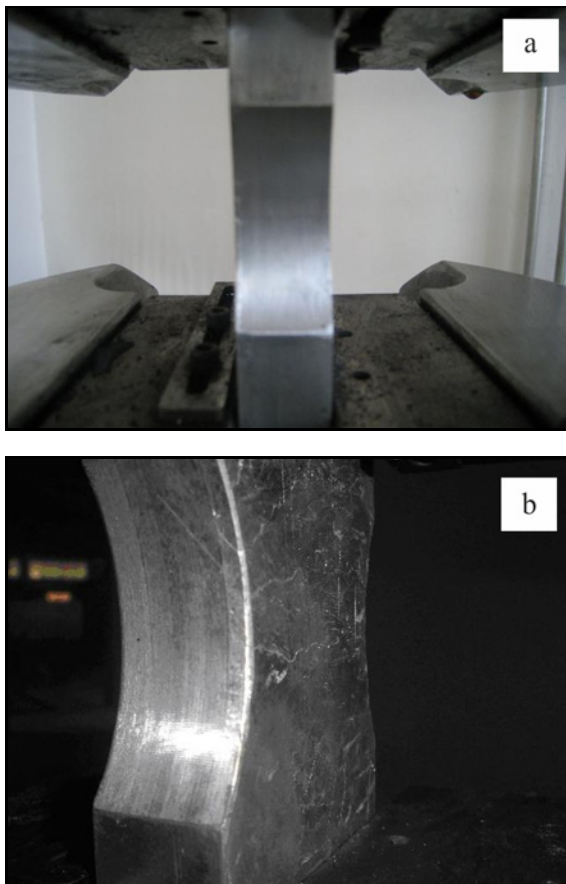


Fig. 7. Before loading (a), after 2e6 cycles (b).

failure in the pure aluminum layer. If $\sigma_a = 48.18$ MPa and for 2 million cycles, the pure aluminum layer of the clad plate exhibits plastic deformation. The interface between the pure aluminum layer and the composite can be clearly seen, as shown in Figs. 7a,b. However, no macroscopic cracks were observed in the specimen. It is concluded that the fatigue life of the specimen is more than 2 million cycles at this stress amplitude, and the interfacial bonding between the materials of the clad plate is good, and there is no unstable failure. Under the same stress state, the life of the specimen is 1.2 million times that at $R = -1$ and 370 000 times that at $R = 0$. It is evident that the mean compressive stress inhibits the initiation of the crack and increases the fatigue strength and fatigue life, which is consistent with the results of the monolithic metal material. Here it is worth pointing out that from Fig. 7, one can see that the cracks start at the edge of the specimen. This happens perhaps because the sample preparations, and especially, machining of the specimen may affect the above results.

A lap-welded specimen of the clad plate was used in the tests. The base metal of the specimen is a composite clad plate, and the butt weld is located in the middle of the specimen. The length of

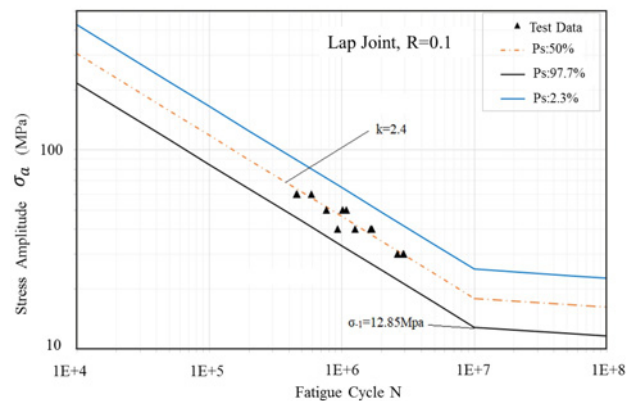


Fig. 8. The stress-life curve of the lap-welded specimen.

the pure aluminum layer cover plate on the pure aluminum layer side of the butt joint is 70 mm, the thickness is 4 mm, and the width is the same as that of the clad plate. The material is a 1060 pure aluminum layer, and the two ends of the pure aluminum layer cover are welded together with the pure aluminum layer of the clad plate to form a lap-welded structure. Therefore, this specimen has three welds; one is the butt-welded joint of the clad plate, and the other two lap welds are located between the pure aluminum layer cover plate and the pure aluminum layer of the clad plate. The main purpose of this lap weld is to protect the composite filler of the butt weld from concentrated nitric acid corrosion; this specimen is called the lap-welded specimen of the clad plate.

A four-point bending fatigue test was carried out on the lap-welded specimen of the clad plate. A Zwick/Roell high-frequency fatigue testing machine was used. During the test, the frequency of the specimen was measured to determine if fatigue fractures had occurred. When the frequency of the specimen exceeds a certain range, it is considered that the specimen has fractured, and the test machine stops the loading. The loading applied is the four-point bending loading method. The test frequency is 70 Hz, the stress ratio is $R = 0.1$, and the test is carried out at room temperature. The two supporting points on the lower side are holding points and the two supporting points on the upper side are loading points.

The test results are shown in Fig. 8. A regression analysis indicates that the slope of the median $S-N$ curve of the lap joints is $k = 2.44$; this curve is steeper than the $S-N$ curve of the welded joints of the monolithic layer alloy. The logarithmic life of the specimen has a normal distribution, and the standard deviation $s = 0.0729$ of the life distribution is slightly larger than the standard deviation of 0.069 in the IIW standard. By subtracting 2 standard deviations from the median



Fig. 9. The typical failure mode of the lap-welded specimen.

curve, the $S-N$ curve with a survival rate of 97.7% can be obtained, and the fatigue limit at $1e7$ cycles is 12.85 MPa. Usually, the fatigue life of a welded joint under a bending fatigue load is longer than that of a tensile-compression load. This is mainly due to the different stress gradients which are perpendicular to the surface of the weld toe. However, with the increase in the plate thickness, the fatigue strength under bending load is more influenced by the size effect, and the fatigue life is reduced faster. When the thickness of the plate is more than 20 mm, the fatigue life under both bending and tensile-compression load tends to be consistent [27]. Therefore, the 97.7% reliability $S-N$ curve of the lap-welded specimen can be used as the design curve for the fatigue strength design of the tank car. The fatigue test includes only the medium- and short-life test data. Similarly, according to the $S-N$ curve of welded joints in the IIW standard, the $S-N$ curve of the lap joint of the composite clad plate is extended to the long-life range, which is used to determine the fatigue strength of the tank car. Like the base composite clad plate, the slope of the long-life range is changed to $k^* = 22$.

The fatigue failure of the lap joint specimen of the composite clad plate is shown in Fig. 9. The fracture of the specimen occurs at the lap weld of the pure aluminum layer cover and the clad plate. The fatigue crack originates from the weld toe position of the pure aluminum layer cover and clad plate, indicating that the lap weld is the weakest area of the specimen. It is observed that the crack begins at the toe of the lap weld and then extends along the cross-section toward the pure aluminum layer. After the failure of the pure aluminum layer, it extends along the cross-section through the interface towards the direction of the composite layer and results in the final fracture of the specimen. There is no peeling at the interface between the pure aluminum layer and the composite

layer, which is different from the tensile fatigue test result of the base metal. In addition to the difference in the crack growth rate between the two materials, the failure mode of the lap-welded specimen is consistent with the failure mode of the welded joint of the single-layer alloy; this also indicates that the form of the $S-N$ curve is the same as that in the IIW standard.

4. Fatigue analysis

During the operation of the tank car carrying concentrated nitric acid, the fatigue load changes over time. Because of different vehicle operating conditions, the form and condition of the railway line and the load vary greatly. At present, the fatigue strength design of tank cars is referred to the AAR Manual of Standards and Recommended Practices, Section C-M1001 Design, Fabrication, and Construction of Freight Cars [28]; the manual defines the load spectrum for a 100-t tank car. This is a three-dimensional spectrum obtained from actual vehicle operating tests using the rain-flow counting method. It is the basis of the fatigue reliability design of tank cars and includes the maximum and minimum load combinations in each group and the number of cycles that appear in this combination.

According to the AAR load spectrum, the fatigue life of tank cars is determined by several fatigue loads, which are the load of the center plate, the load of the side bearing, the longitudinal and vertical loads of the coupler, and the torsional load. The center plate bears the vertical load of the tank car, including its weight and load of the tank. The side bearing load is caused by the side roll movement of the tanker during operation. When the two sides of the bogie side bearing roll in different directions, the car experiences a torsional load. In addition, the standard also considers the proportional mileage of empty to loaded tank car.

4.1. Analysis of fatigue failure mode

The fracture of specimen occurs at the lap weld of the pure aluminum cover and the clad plate. The fatigue crack originates from the weld toe position of the pure aluminum cover and clad plate, indicating that the lap weld is the weakest area of the specimen.

The propagation mode of the crack of the lap-welded specimen is shown in Fig. 10. It is observed that the crack begins at the toe of the lap weld and then extends along the cross-section toward the pure aluminum layer. After the failure of the pure aluminum layer, it extends along the cross-section through the interface towards the direction of the Al-Mg alloy layer and results in the final fracture of the specimen. There is no peeling at the interface between the pure aluminum layer and the Al-Mg alloy

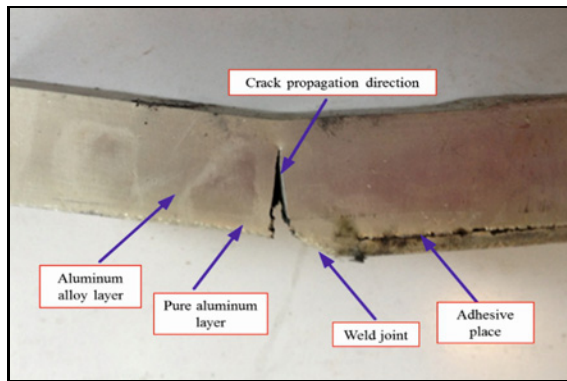


Fig. 10. Crack propagation of lap-welded specimen.

layer, which is different from the tensile fatigue test result of the base metal. In addition to the difference in the crack growth rate between the two materials, the failure mode of the lap-welded specimen is consistent with the failure mode of the welded joint of the single aluminum alloy, which also indicates that the form of the $S-N$ curve is the same as that in the IIW standard.

4.2. Evaluation method

Based on the structural and mechanical similarity, it is assumed that there is a linear relationship between a load of a tank car and its weight [28–30]. The load spectra of a 100-t empty and loaded tank car used in the AAR standard are converted into the load spectra of a 70-t empty and loaded tank car in this study. Due to the linear relationship between the load and the stress on the tank car, a stress analysis of the tank car body under several loads is carried out firstly, and the major stress areas are identified to determine the source of the fatigue. Second, the load spectra of the tank car are transformed into the stress spectra of the large stress positions under these load spectra. The transformation of the load spectra and stress spectra is based on the assumption of a linear relationship between the load and the stress, as shown in the following formula:

$$\sigma_t/P_t = \sigma_i/P_i, \quad (2)$$

where P_t is the load in the load spectrum of the car and σ_t is the stress on the part of the car receiving the load spectrum P_t . P_i is the load exerted by the finite element calculation, and σ_i is the stress on the car body under the action of the load P_i .

Considering the load spectrum conversion for tank cars with different weights, the load spectrum of the 70-t tank car is as follows:

$$\sigma_t = \alpha P_t \times \sigma_i/P_i, \quad (3)$$

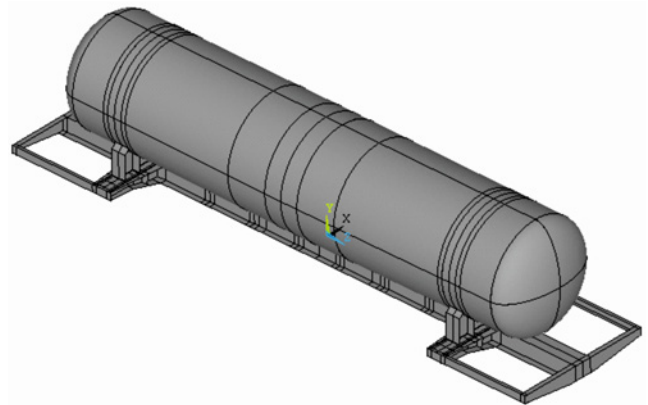


Fig. 11. Geometric structure of the tank car.

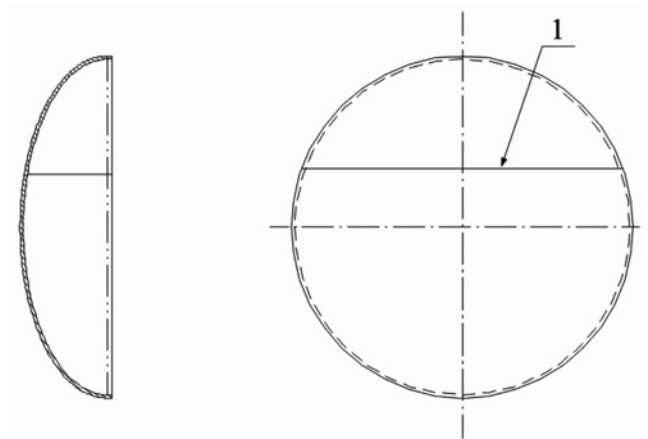


Fig. 12. Weld seam position on the dome.

where α is a conversion coefficient of the load spectrum.

After the stress spectrum of the key positions is obtained, the fatigue damage of these key positions under vertical, longitudinal, torsional, and rolling fatigue loads was calculated combined with the fatigue performance data of the base metal and lap joints of the composite cladded plate. According to the Miner linear cumulative damage theory, the total damage to the key positions of the tank car body is determined.

4.2. Finite element analysis

The 70-t tank car carrying concentrated nitric acid is a bearing structure, and it consists of the tank body and the bottom frame. The tank body is a horizontal tube structure welded by butt joints from the cylinder body and the head; the tank material is the composite cladded plate. The bottom frame consists of a center sill, bolster end beams, and short side beams. The structure of the 70-t tanker is shown in Fig. 11. The vehicle weight is less than 23 t, and the load is greater

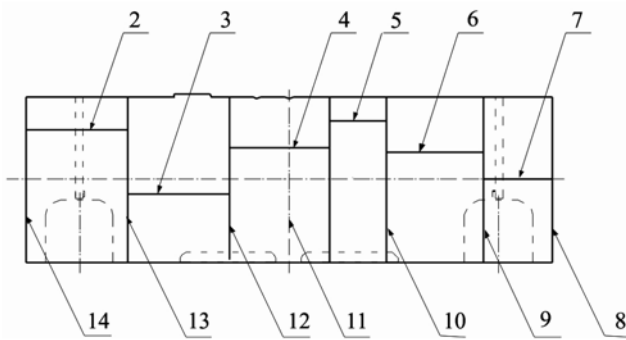


Fig. 13. Weld seam positions on the barrel.

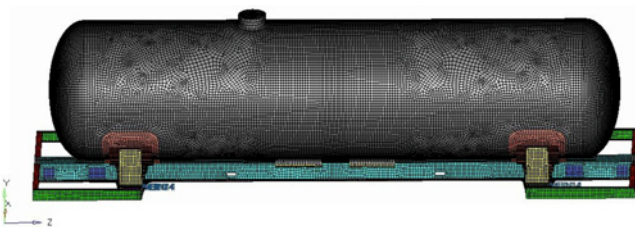


Fig. 14. Finite element model of the tank car.

than 70 t, improving transportation efficiency.

The front and back heads consist of spherical convex panels that are hot-pressed using the two plates, as shown in Fig. 12. The six longitudinal welds in the cylinder are marked as 2 to 7, and the seven circumferential welds (including the two welds of the head seal) are marked as 8 to 14. Fillet welding is used to join the circumferential welds and the longitudinal welds, as shown in Fig. 13. The butt weld joint is double sides fully penetrated, with a pure aluminum layer cover plate that protects the inside from corrosion.

The finite element model is shown in Fig. 14. There are 68240 elements and 68353 nodes in the model. Solid45 element is used to simulate the stow-wood, and the other structures are simulated by Shell181 element. The surface contact is established between the tank body and the stow-wood and between the stow-wood and the underframe; the constraints of the center plate and side bearing are simplified as elastic constraints. In the model, the X -direction is the transverse direction, the Y -direction is vertical, and the Z -direction is longitudinal; the tank body material is the composite cladded plate. The material parameters are set up based on the elastic-plastic analysis results of the composite cladded plate. The material of the frame is steel.

The finite element analysis of the tank car body is conducted using ANSYS. Vertical load, coupler longitudinal load, torsional load, and rolling load leading to side bearing loading are applied to the tank car body. The stresses of the tank body under different

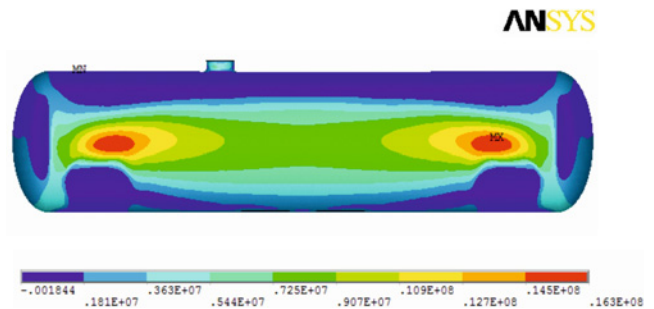


Fig. 15. Principal stress distributions of the tank body under a vertical load. Note: the unit of the given numbers is MPa.

load cases are analyzed. Elastic restraint is applied to the center plate for the vertical, longitudinal, and torsional load cases. Elastic restraint is also applied to the side bearing for the rolling load case. The principal stress distribution under vertical loads (710 kN) is shown in Fig. 15. From this figure, one can see that the stress for the different specimens is different, e.g., it is 16.3 MPa for Support 1 and 14.6 MPa for Weld 13, as shown in Table 3. It is evident that relatively high stress occurs near the support. In this analysis, only the fatigue damage of the tank body is evaluated, not considering the underframe and saddle, according to the stress distribution of the tank car body under different load cases. Totally 4 positions in the base material, which are near the tank support, and 4 weld positions are identified as the key positions of fatigue evaluation. The stress values of the key positions under the four load conditions were taken from finite element analysis, and then the stress value was divided by the load, the load stress transfer coefficients were determined (Table 3).

Based on the load spectrum of the empty and loaded tank car in the AAR standard and the stress transfer coefficients of the key positions, the stress spectrum of the key positions under different load cases is obtained using Eq. (3). The test mileage is 11 148 miles, and 7 139 031 stress cycles occurred. The corresponding damage values were calculated based on the $S-N$ curves of the base metal and the lap joints of the composite cladded plate; the damage values of the key locations under various load cases of the empty and loaded tank car are shown in Table 4. It is evident that the damage caused by the rolling load and torsional load can be neglected. The longitudinal load causes most of the damage, and the maximum damage occurred at the position, which is the lowest point of the cross-section of the tank body support.

The mileage proportion of an empty tank car to a loaded car in the AAR standard is 93 %. According to the mileages of the load spectrum of the empty and loaded car, the damage under the load spectrum is converted to the damage per unit of mileage. Subse-

Table 3. Load-stress transfer coefficients of key points

Position	Description	Vertical load (710 kN)		Roll load (233 kN m)		Longitudinal load (207 kN)		Torsional load (304 kN m)	
		Stress (MPa)	Coefficient (MPa)/(kN)	Stress (MPa)	Coefficient (MPa)/(kN)	Stress (MPa)	Coefficient (MPa)/(kN)	Stress (MPa)	Coefficient (MPa)/(kN)
1	Support1	16.3	0.02296	6.98	0.02993	2.35	0.0114	7.67	0.0252
2	Support2	9.05	0.01274	14.1	0.06045	2.02	0.0098	9.47	0.0312
3	Support3	2.31	0.00325	4.63	0.01985	14.9	0.0724	3.51	0.0115
4	Support4	5.73	0.00807	5.03	0.02157	3.12	0.0151	20.5	0.0674
5	Tank body3	12.8	0.01802	3.01	0.01290	1.9	0.00919	5.09	0.01674
6	Tank body7	15.9	0.02239	6.97	0.02988	0.622	0.00300	7.68	0.02526
7	Tank body9	11.5	0.01619	6.08	0.02606	2.19	0.01059	4.94	0.01625
8	Tank body13	14.6	0.02056	6.65	0.02851	2.19	0.01059	6.65	0.02187

Support1-Upper corner of the support; Support2-Corner of support.

Table 4. Damages at the key points under different loads

Position	Loaded car				Empty car			
	Vertical	Rolling	Longitudinal	Torsional	Vertical	Rolling	Longitudinal	Torsional
Support1	0	0	0.867E-07	0	0	0	0	0
Support2	0	0	4.42E-09	0	0	0	0	0
Support3	0	0	4.16E-03	0	0	0	1.78E-03	0
Support4	0	0	5.48E-07	0	0	0	0.842E-07	0
Tank body3	0.106E-07	0	1.08E-06	0	0	0	2.63E-07	0
Tank body7	4.34E-07	0	0	0	0	0	0	0
Tank body9	0	0	2.11E-06	0	0	0	4.43E-07	0
Tank body13	1.93E-07	0	2.11E-06	0	0	0	4.43E-07	0

Table 5. Buckling strength of numerical results

Position	Total damage	Fatigue life (10 000 km)
Support1	4.03E-12	3.99E+07
Support2	2.05E-13	7.83E+08
Support3	2.73E-07	590
Support4	2.92E-11	5.50E+06
Tank body3	6.25E-11	2.58E+06
Tank body7	2.02E-11	7.98E+06
Tank body9	1.18E-10	1.37E+06
Tank body13	1.27E-10	1.27E+06

quently, the total damage per unit of the mileage of the key positions of the tank body can be obtained by linear accumulation. The total damage determined the fatigue life. Table 5 shows the total damage per unit of mileage and fatigue life of the key positions of the tank body. The minimum fatigue life of the base material is 5.9 million km, and the minimum fatigue life of the weld is 1270 million km, which are all longer than the design life of 2.5 million km. Therefore, the fatigue strength of the 70-t tank car consisting of the composite clad material meets the requirements.

Finally, it should be pointed out that in the present

finite element analysis of the tank car body, during the simulations, the vertical load, coupler longitudinal load, torsional load, and rolling load were applied, and these loads were applied separately in the subsequent simulation variants. However, the simultaneous occurrence of the mentioned load variants can lead to more complicated stress distributions, which may have a significant impact on the results of calculations, in particular, for the prediction of mechanical behavior. For example, under these complex loads, the yielding may also occur on the pure aluminum layer, but the plastic deformation may be caused on the Al-Mg alloy

layer, and even the pure aluminum layer may exhibit necking.

5. Conclusions

The heavy load and transportation safety of tank cars carrying concentrated nitric acid has attracted increased attention. The use of composite clad composites can solve the problems associated with the corrosion and lack of strength of tank car bodies. Static strength analyses and fatigue strength tests of a composite laminate plated are conducted, and the fatigue strength design of a 70-t tank car constructed using the composite is investigated.

1. Finite element analysis is used to simulate the tensile test of the clad plate. The stress and strain behavior of the composite clad plate under tensile load is determined, and the macro-mechanical performance parameters of the clad plate are calculated. Under tensile load, the pure aluminum layer yields first, and the load is then supported by the composite layer without the occurrence of plastic deformation. The pure aluminum layer does not exhibit necking, and the composite clad plate achieves a high strength value.

2. Fatigue tests of the composite clad plate using $R = -1$, $R = 0$, and $R = -\infty$ are carried out, and the $S-N$ curve with a survival rate of 97.7% is determined. The curve slope is 5.2, which is basically the same as that of the monolithic layer alloy. The fatigue limit corresponding to the $1e7$ cycle is 23.62 MPa, which is much higher than the fatigue limit of 11 MPa for the pure aluminum layer. The mean tensile stress reduces the fatigue strength, and the mean compressive stress increases the fatigue strength, which is in line with the Goodman correction method. Fatigue cracks first occur at the edge of the pure aluminum layer and are accompanied by interfacial delamination, extending along the cross-section to the pure aluminum layer. After the pure aluminum layer is damaged, the cracks expand along the transverse section towards the composite and result in the final fracture of the specimen.

3. The $R = 0.1$ four-point bending fatigue test of the lap-welded specimen of the composite clad plate is carried out. The $S-N$ curve with a survival rate of 97.7% is obtained, and the fatigue limit corresponding at the $1e7$ cycle is 12.85 MPa. The fatigue crack originates from the weld toe of the lap weld and first extends along the transverse section to the pure aluminum layer. After the failure of the pure aluminum layer, the specimen is finally fractured in the direction of the composite layer along the cross-section and through the interface. The interface between the pure aluminum layer and the composite layer has not been stripped.

4. The finite element method is used to calculate the stress state under the typical load cases of the tank body carrying concentrated nitric acid. Based on the load spectrum of the tank car in the AAR standard, the load spectrum of the center plate, the side bearing, and the coupler are transformed into the stress spectrum of the key positions of the tank car body. The fatigue life of the key positions of the tank car body is estimated according to the Miner linear cumulative damage theory based on the $S-N$ curve of the composite clad plate base metal and the lap-welded specimen. The minimum life of the key point of the base material is 5.9 million km, and the minimum life of the key point of the weld is 1270 million km, which is longer than the design life of 2.5 million km. This indicates that the fatigue strength of the 70-t tank car constructed with the composite clad material meets the safety requirements.

Based on the above experimental results and finite element analysis on the fatigue performance, failure analysis, and fracture mechanism, the sealing status of the transformer oil tank can be monitored and evaluated very effectively, which can further be used for the fault diagnosis and failure analysis under various conditions such as normal operations, transformer lifting, and transportation.

Acknowledgements

This research was supported in part by the National Key Research and Development Project of China (Grant number: SQ2020YFF0417369), Public Welfare Technology Research Program of Zhejiang Province under Grant number LGG20E050004, and Major Projects of Science and Technology Innovation 2025 of Ningbo (Grant numbers: 2020Z115, 2021E006, and 2020Z077).

References

- [1] M. R. Saat, C. P. Barkan, Generalized railway tank car safety design optimization for hazardous materials transport: Addressing the trade-off between transportation efficiency and safety, *J. Hazard. Mater.* 189 (2011) 62–68. [doi:10.1016/j.jhazmat.2011.01.136](https://doi.org/10.1016/j.jhazmat.2011.01.136)
- [2] C. P. Barkan, S. V. Ukkusuri, S. T. Waller, Optimizing the design of railway tank cars to minimize accident-caused releases, *Comput. Oper. Res.* 34 (2007) 1266–1286. [doi:10.1016/j.cor.2005.06.002](https://doi.org/10.1016/j.cor.2005.06.002)
- [3] D. Lesuer, C. Syn, O. Sherby, J. Wadsworth, J. Lewandowski, W. Hunt, Mechanical behaviour of laminated metal composites, *Int. Mater. Rev.* 41 (1996) 169–197. [doi:10.1179/imr.1996.41.5.169](https://doi.org/10.1179/imr.1996.41.5.169)
- [4] P. Partridge, I. Farrow, D. Smith, Advanced composite metallic laminates, *Mater. Sci. Technol.* 10 (1994) 531–535. [doi:10.1179/mst.1994.10.6.531](https://doi.org/10.1179/mst.1994.10.6.531)
- [5] Y. Wu, B. Feng, Y. Xin, R. Hong, H. Yu, Q. Liu, Microstructure and mechanical behavior of an Mg

- AZ31/Al 7050 laminate composite fabricated by extrusion, *Mater. Sci. Eng. A* 640 (2015) 454–459. [doi:10.1016/j.msea.2015.05.094](https://doi.org/10.1016/j.msea.2015.05.094)
- [6] X. P. Zhang, M. J. Tan, T. H. Yang, J. T. Wang, Isothermal rolling of Mg-based laminated composites made by explosion cladding, *Key Engineering Materials* 443 (2010) 614–619. [doi:10.4028/www.scientific.net/KEM.443.614](https://doi.org/10.4028/www.scientific.net/KEM.443.614)
- [7] B. Liu, L. Huang, L. Geng, B. Wang, C. Liu, W. Zhang, Fabrication and superior ductility of laminated Ti-TiBw/Ti composites by diffusion welding, *J. Alloys Compd.* 602 (2014) 187–192. [doi:10.1016/j.jallcom.2014.02.140](https://doi.org/10.1016/j.jallcom.2014.02.140)
- [8] R. Jamaati, M. R. Toroghinejad, Investigation of the parameters of the cold roll bonding (CRB) process, *Mater. Sci. Eng. A* 527 (2010) 2320–2326. [doi:10.1016/j.msea.2009.11.069](https://doi.org/10.1016/j.msea.2009.11.069)
- [9] Z. Wang, L. Zhai, M. Ma, H. Yuan, W. Liu, Microstructure, texture and mechanical properties of Al/Al laminated composites fabricated by hot rolling, *Mater. Sci. Eng. A* 644 (2015) 194–203. [doi:10.1016/j.msea.2015.07.035](https://doi.org/10.1016/j.msea.2015.07.035)
- [10] J. Wittenauer, O. Sherby, Factors influencing the fatigue behavior of ferrous laminates, *J. Eng. Mater. Technol.* 109 (1987) 244–251. [doi:10.1115/1.3225971](https://doi.org/10.1115/1.3225971)
- [11] F. Kümmel, T. Hausöl, H. W. Höppel, M. Göken, Enhanced fatigue lives in AA1050A/AA5005 laminated metal composites produced by accumulative roll bonding, *Acta Mater.* 120 (2016) 150–158. [doi:10.1016/j.actamat.2016.08.039](https://doi.org/10.1016/j.actamat.2016.08.039)
- [12] R. Pippan, K. Flechsig, F. Riemelmoser, Fatigue crack propagation behavior in the vicinity of an interface between materials with different yield stresses, *Mater. Sci. Eng. A* 283 (2000) 225–233. [doi:10.1016/S0921-5093\(00\)00703-6](https://doi.org/10.1016/S0921-5093(00)00703-6)
- [13] J. Cui, Y. Fu, N. Li, J. Sun, J. He, Study on fatigue behavior of metal/metal laminates, *Acta Metall. Sin.* 36 (2000) 268–271. [doi:10.3321/j.issn:0412-1961.2000.03.011](https://doi.org/10.3321/j.issn:0412-1961.2000.03.011)
- [14] J. W. He, M. Jia, S. P. Wen, N. Li, Cracking in the soft interface layer of an Al-alloy laminate, *Int. J. Fatigue* 25 (2003) 421–426. [doi:10.1016/S0142-1123\(02\)00164-0](https://doi.org/10.1016/S0142-1123(02)00164-0)
- [15] O. Kolednik, J. Predan, F. D. Fischer, P. Fratzl, Improvements of strength and fracture resistance by spatial material property variations, *Acta Mater.* 68 (2014) 279–294. [doi:10.1016/j.actamat.2014.01.034](https://doi.org/10.1016/j.actamat.2014.01.034)
- [16] I. Szachogluchowicz, L. Sniezek, V. Hutsaylyuk, Low cycle fatigue properties of AA2519-Ti6Al4V laminate bonded by explosion welding, *Eng. Failure Anal.* 69 (2016) 77–87. [doi:10.1016/j.engfailanal.2016.01.001](https://doi.org/10.1016/j.engfailanal.2016.01.001)
- [17] I. Szachogluchowicz, L. Sniezek, V. Hutsaylyuk, Low cycle fatigue properties laminate AA2519-Ti6Al4V, *Procedia Eng.* 114 (2015) 26–33. [doi:10.1016/j.proeng.2015.08.022](https://doi.org/10.1016/j.proeng.2015.08.022)
- [18] L. Wei, D. Wang, Effect of ultrasound-assisted vibration on Ti-6Al-4V/Al2024-T351 laminated material processing with geometric tools, *Int. J. Adv. Manuf. Technol.* 106 (2020) 219–232. [doi:10.1007/s00170-019-04637-7](https://doi.org/10.1007/s00170-019-04637-7)
- [19] C. Alía, J. M. Arenas, J. C. Suárez, P. Pinilla, Mechanical behaviour of vinylester adhesive joints used in laminated material for steel structures, *Mar. Struct.* 69 (2020) 102687. [doi:10.1016/j.marstruc.2019.102687](https://doi.org/10.1016/j.marstruc.2019.102687)
- [20] Y. Huang, J. Liu, X. Huang, J. Zhang, G. Yue, Fatigue crack growth and delamination behaviours of advanced Al-Li alloy laminate under single tensile overload, *Fatigue Fract. Eng. Mater. Struct.* 39 (2016) 47–56. [doi:10.1111/ffe.12319](https://doi.org/10.1111/ffe.12319)
- [21] GB/T 16475: Temper Designation System for Wrought Aluminium and Aluminium Alloy, 1996.
- [22] C. M. Sonsino, Course of SN-curves especially in the high-cycle fatigue regime with regard to component design and safety, *Int. J. Fatigue* 29 (2007) 2246–2258. [doi:10.1016/j.ijfatigue.2006.11.015](https://doi.org/10.1016/j.ijfatigue.2006.11.015)
- [23] A. Hobbacher, Recommendations for fatigue design of welded joints and components, International Institute of Welding, IIW-1823-07 ex. XIII-2151r4-07/XV-1254r4-07, Paris, France, 2008.
- [24] JB/T 4734: Aluminium Welded Vessels, 2002.
- [25] ASME Boiler & Pressure Vessel Code, Section II, Part D, 2004.
- [26] S. Maddox, Fatigue design optimisation in welded joints, *Advances in Fatigue Science and Technology*, Springer, Dordrecht, 1989, pp. 551–568. [doi:10.1007/978-94-009-2277-8_25](https://doi.org/10.1007/978-94-009-2277-8_25)
- [27] Manual of Standards and Recommended Practices Section C-Part II, Design, Fabrication, and Construction of Freight Cars, 2011.
- [28] C. Sheng, Fatigue life analysis of freight car based on AAR standard, *Mod. Manuf. Eng.* 3 (2014) 44–51. [doi:10.3969/j.issn.1671-3133.2014.03.012](https://doi.org/10.3969/j.issn.1671-3133.2014.03.012)
- [29] S. Qu, P. B. Wu, Z. H. Liu, The Application of AAR load spectrums in the fatigue assessment for G70 tank tarbody, *Advanced Materials Research* 690–693 (2013) 1960–1965. [doi:10.4028/www.scientific.net/AMR.690-693.1960](https://doi.org/10.4028/www.scientific.net/AMR.690-693.1960)
- [30] Y. N. Lai, Fatigue analysis of C₈₀(B) freight train, *Mach. Des. Manuf.* 8 (2015) 105–109. [doi:CNKI:SUN:JSYZ.0.2015-08-029](https://doi.org/10.1016/j.cnki:sun.jsyz.0.2015-08-029)